RESEARCH ARTICLE | APRIL 30 2024

Performance analysis of a modified Allam cycle combined with an improved LNG cold energy utilization method

Yi Wu; Zheng Wang; Yafei Liu; Qinghe Guo; Zhangquan Wen; Dan Chen; Kaigang Gong;
Peiwang Zhu; Gang Xiao

J. Renewable Sustainable Energy 16, 024703 (2024)
https://doi.org/10.1063/5.0202719

Journal of Renewable and Sustainable Energy ARTICLE pubs.aip.org/aip/rse

Performance analysis of a modified Allam cycle combined with an improved LNG cold energy utilization method

Cite as: J. Renewable Sustainable Energy **16**, 024703 (2024); doi: 10.1063/5.0202719
Submitted: 6 February 2024 · Accepted: 16 April 2024 ·
Published Online: 30 April 2024

View Online Export Citation CrossMark

Yi Wu,[1,2,a] Zheng Wang,[1,2,a] Yafei Liu,[1,2,a] Qinghe Guo,[1,2,a] Zhangquan Wen,[1,2,a] Dan Chen,[1,2,a] Kaigang Gong,[1,2,a] Peiwang Zhu,[1,2,a] and Gang Xiao[1,2,b]

AFFILIATIONS

[1]Key Laboratory of Clean Energy and Carbon Neutrality of Zhejiang Province, Zhejiang University, Hangzhou, Zhejiang 310027, China
[2]State Key Laboratory of Clean Energy Utilization, Zhejiang University, 38 Zheda Road, Hangzhou, 310027, China

[a]**Electronic addresses:** 22127052@zju.edu.cn; 11927096@zju.edu.cn; 12027088@zju.edu.cn; guo-qinghe@zju.edu.cn; 12227078@zju.edu.cn; 22227126@zju.edu.cn; 12327144@zju.edu.cn; and zhupw@zju.edu.cn
[b]**Author to whom correspondence should be addressed:** xiaogangtianmen@zju.edu.cn

ABSTRACT

The Allam cycle is a promising power cycle that could achieve 100% carbon capture as well as high efficiency. In order to further enhance system operating performance, here we propose a modified Allam cycle with an improved liquified natural gas (LNG) cold energy utilization method. The flow rate fluctuation of LNG is suppressed by variable speed adjustment of the air compressor, and the cold energy of LNG is transferred to liquid oxygen, which could implement a stable cold energy supply. The whole process is modeled including air separation unit and LNG supply path. Furthermore, the system thermodynamic and economic performance is evaluated through parametric analysis, and the proposed system superiority is highlighted by comparing with conventional Allam-LNG cycle. The results indicate that the system could achieve 70.93% of net thermal efficiency, 65.17% of electrical efficiency, and \$403.63 million of net present value, which performs 5.76% and 6.48% enhancement of efficiency and 11% improvement of economic revenue. Moreover, the system off-design operation is assessed; 87% to 100% of compressor speed adjustment range is determined that could cope with −13% to 9% of LNG flow rate fluctuation.

I. INTRODUCTION

With the increasing focus on the greenhouse effect, all the world's leading economies had drawn up their target of carbon neutrality. However, according to the international energy agency, the global energy-related CO_2 emissions reached 36.8 Gt in 2022, a new high of all-time. Emissions produced by fossil fuel combustion from electricity and heat generation still takes the largest proportion of 39.7%.[1] Although considerable renewable power plants were invested and constructed, conventional energy resources still play an important role in a foreseeable future.[2] Therefore, oxy-fuel combustion technology with carbon capture is a perspective solution for electricity generation. Among them, the Allam cycle has received much attention, which is featured with semi-closed configuration, pure oxygen combustion, and highly CO_2 concentration. As the result, 100% of CO_2 could be theoretically captured in pipeline.[3] The pure oxygen is fed by air separation unit, along with compression heat fed to recuperator. Moreover, the Allam cycle could achieve nearly zero pollution and higher efficiency than other fossil-fueled power plants, due to the use of natural gas as fuel and higher working temperature. Considering the advantages of Allam cycle, the demonstration project is being commercialized by NET power in Texas in recent years, with the partnership of Toshiba corporation.[4]

Extensive investigations have been carried out on Allam cycle, mainly aimed at system optimization and component design. Rogalev *et al.*[5] developed an optimized sCO_2 turbine model, and the preliminary design parameters of rotor are conducted based on a 50 MW prototype power plant; the operating results showed a good energy and economic performance. Peng *et al.*[6] studied the ignition effect of C_2H_4 diluted in CO_2/O_2 environment experimentally, under the pressure range from 1 and 10 atm. Liu *et al.*[7–10] conducted a series of comprehensive research, to explore the chemical effect of flame diluted with CO_2. In terms of system evaluation, Ebadi *et al.*[11] compared the thermodynamic performance between the Allam cycle and sCO_2 Brayton cycle, and the results showed that the Allam cycle could exhibit higher efficiency at lower pressure ratio, as the working fluid can be heated to higher temperature in combustion chamber. Haseli and Sifat[12] developed an integrated system of Allam cycle and air separation unit, where heat integration and oxygen supply is considered, and the operating parameters are conducted and net cycle efficiency reached to 58.2% after optimization. Amann *et al.*[13] evaluated the oxy-fuel system performance when integrated into ASU, at least 6% efficiency penalty is found, which further increases with higher purity of oxygen produced. Based on steady simulation, the dynamic simulation was also developed by Fernandes *et al.*,[14] who conducted a comprehensive control strategy on Allam cycle integrated with an ASU, to reject disturbances caused by natural gas composition variation. Zaryab *et al.*[15] also established a load change model of Allam cycle; in his work, detailed control strategy is proposed and response characteristic is investigated.

In order to further improve the Allam cycle thermodynamic and economic performance, lots of newly configured cycle patterns and operating methods are developed. Reheat path is added to the system by Chan *et al.*[16] to increase the power output. Xie *et al.*[17] utilized multi-compressor to store energy through compression refrigeration; the author also came up with an Allam cycle-heat pump combined cycle,[18] which is an alternative way utilizing CO_2 compression heat to generate energy. Dokhaee *et al.*[19] integrated the lithium bromide absorption cooling cycle with the exhaust heat of CO_2 at the outlet of recuperator, to raise the exergy efficiency of system. Luo *et al.*[20] developed a syngas-gas fired Allam cycle and analyzed the exergy destruction in main components, while concentrated solar energy gasifier is integrated into the coal gasification process by Xin *et al.*[21] Zhu *et al.*[22] proposed a modified Allam cycle called "Allam-Z cycle," the modified cycle with lower turbine inlet temperature at 700 °C and higher exhaust pressure at 7.2 MPa, that the working fluid could be condensed by cooling water directly. The results showed significant superiority when compared with power cycle under the same turbine inlet temperature, resulting from the pressure raise is proceed by pump instead of compressor. Similar configuration also adopted by Fu,[23] in his work, a biomass gasification unit is coupled and CO_2 is directly condensed at 20 °C, the result delivered an 11.2% improvement compared with original cycle. However, low turbine inlet temperature and pressure ratio hinder the efficiency enhancement of "Allam-Z" cycle.

The Allam cycle combined with liquid natural gas (LNG) cold energy utilization could be regarded as the further optimization of Allam cycle on power output and energy efficiency, considering that lower condensation temperature could be achieved and turbine inlet parameters could further increase. Simultaneously, tons of LNG cold energy could be recovered during regasification.[24] Organic Rankine cycle is currently the most common application to recover cold energy of LNG. Sun *et al.*[25] reviewed the existing LNG cold energy utilization Rankine cycle and categorized them into different kinds. The best working pressure and temperature range for kinds of power cycle are summarized when adopting different working medium. While Ma *et al.*[26] conducted a more detailed comparison of working fluids including pure fluid and mixing fluid. Among various working fluids to recover LNG cold energy, CO_2 is another feasible choice that has a low triple phase point temperature (−53 °C). Wang *et al.*[27] constructed a CO_2 Rankine cycle to recover LNG cold energy. Cao *et al.*[28] developed a cascade sCO_2/CO_2 Rankine cycle that integrated with LNG cold energy; the result indicated that CO_2 is a competitive candidate of working fluids, and the combined cycle delivered levelized cost of electricity less than 0.03 $/kWh. To date, the research on the Allam cycle combined with LNG cold energy is not yet comprehensive; Yu[29] analyzed the feasibility of the integrated system of LNG cold energy and Allam cycle, and the result shows that exergy efficiency has a remarkable enhancement. The author also pointed out that the gasified LNG after releasing cold energy could recycle to combustion chamber as fuel, which can make the full use of cold energy and chemical energy of LNG. Chan *et al.*[30] developed a whole process of cold energy integrated Allam cycle, the steady simulation and exergy destruction in main component is conducted, and the overall energy efficiency achieved to 65.7%. Li *et al.*[31] developed a dual-pressure Allam cycle that combined with LNG cold energy, bifurcated CO_2 flows are condensed at different condensing pressure to reduce heat transfer loss, and the system energy efficiency was improved to 70.22% when extra cooling exergy output is included.

The integrated system that combines with Allam cycle, ASU, and LNG cold energy is quite complex, and the disturbance of single parameters may amplify to the whole integrated system. For instance, the supply of LNG may fluctuate within a certain range, which depends on supply-demand of the industry supply chains,[32] which results in heat transfer deterioration or cavitation in components. However, there has been little investigation and solution to this problem when cold energy is utilized in Allam cycle. Therefore, in this work, a variable compressor speed adjustment method is adopted to model the integrated LNG cold energy utilization Allam cycle. The system thermodynamic and economic performance is analyzed, and the superiority of the system is highlighted by comparison with conventional Allam-LNG cycle. Moreover, the acceptable LNG flow rate fluctuation range is determined, and the result shows our model is capable to offset wide range of fluctuation based on our improved LNG cold energy utilization method.

II. SYSTEM DESCRIPTION

The integrated system could be divided into two subsystems, power cycle and air separation unit, as depicted in Fig. 1. The power cycle is organized by a combustion chamber (CC), gas turbine (T1), recuperator (HX1), water separator (WS1), CO_2 cooler (HX2), splitter, and four liquid circulation pumps (P1–P4). The pure oxygen is added to a CO_2 branch as oxidant flow, which send to combustion chamber with the outlet temperature of 1150 °C. The recycled CO_2 flow is working as supercritical CO_2 Brayton cycle, while the turbine blade cooling is realized by a partial CO_2 bifurcated after P1. The mainstream can reach theoretically 100% purity of CO_2 after WS1, as the combustion product contains only water and CO_2. Carbon capture is accomplished at the outlet of HX2, where pure CO_2 is condensed to liquid for the convenience of collection.

In terms of air separation unit, air after filtration (AF) is first compressed via multistage compressors (C1, C2) with intercooling and drying (WS2, WS3). The compression heat is transferred to HX1 to raise the recycled CO_2 temperature. The compressed air enters the main heat exchanger (HX4), where air is cooled by evaporating LNG and air distillation product. The cooled air stream is throttled into a lower temperature and fed to the high pressures column (HPC) at upper and lower inlet, and the product from the top and the bottom of HPC gets further cooled in HX3 and send to low pressure column (LPC) for second stage distillation. The final cryogenic product includes nitrogen and oxygen. The liquid oxygen with low temperature is pumped to power cycle for cold energy recover and transportation

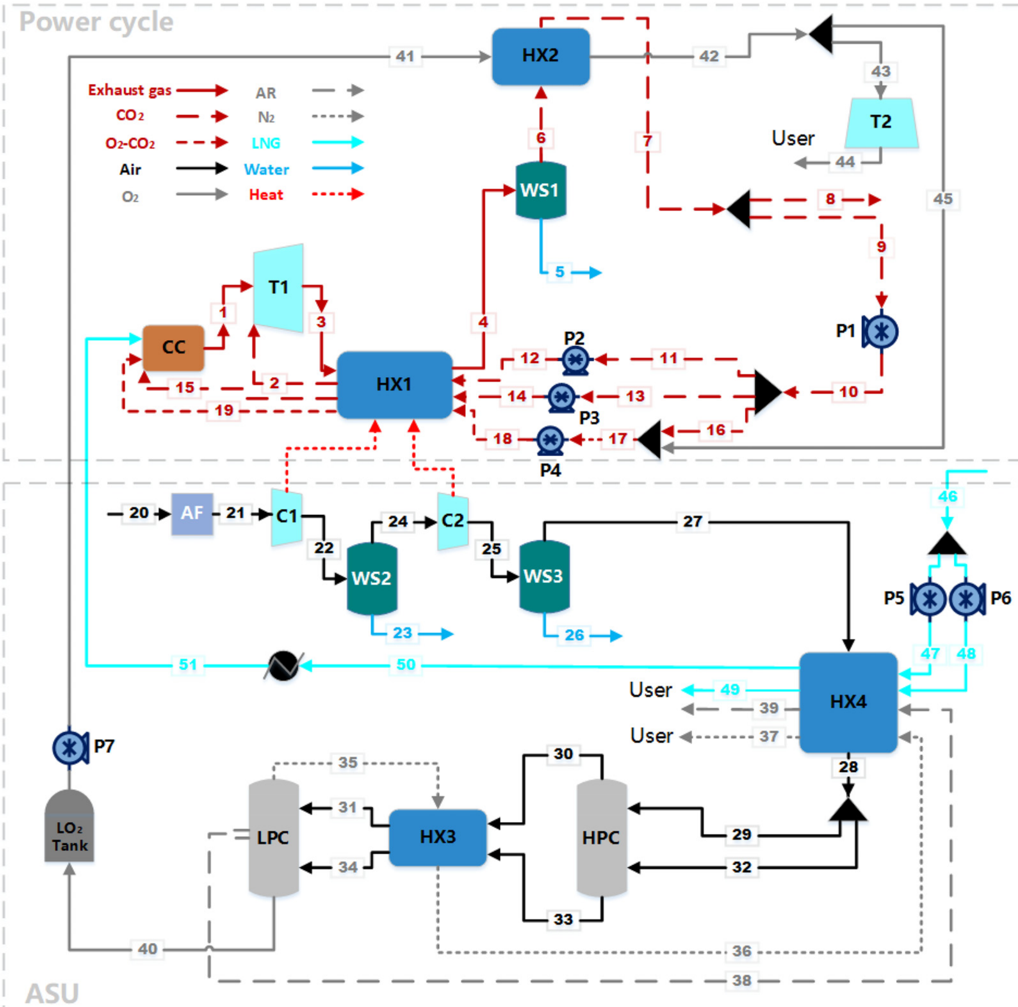

FIG. 1. Schematic diagram of Allam-ASU cascade cold energy utilization integrated system.

in steel cylinder or through pipeline, while nitrogen is distributed to user after cold energy recovery in HX4.

As mentioned above, the heat transfer deterioration may happen in LNG evaporator due to the LNG supply flow rate fluctuation, which may lead to fluid freeze or pump cavitation and increase power cycle operation risk. In order to address this problem, our improved LNG cold energy utilization method could enable a cascade cold energy recovery process, where LNG cold energy is transferred to air product of oxygen and then utilized by power system. The air compressor in ASU adopts the speed-variable operation method, to achieve a pressure adjustable characteristic. Consequently, the LNG flow fluctuation could be offset by the compression-throttling process to maintain a stable distillation path. The compression heat of air compressor is delivered to recuperator of power cycle through thermal oil, which could offer enough heat even at minimum compressor load.

Figure 2 illustrate the pressure-enthalpy diagram of the modified Allam cycle in this work, as well as the reported Allam cycles. The recycled CO_2 in the original Allam cycle is compressed as gaseous state while it is condensed near critical line in Allam-Z cycle. According to the comparison between diagrams, the combination of LNG cold energy with Allam cycle could exhibit higher pressure ratio and more power output. Detailed superiority of the system is further verified on following discussions.

III. MODEL DEVELOPMENT AND METHOD

A. Main components

The modeling of main components is carried out based on their thermodynamics principles and working conditions. The isentropic efficiency η_{is} is adopted to describe the energy conversion process for compressor, pump, and turbine. Isentropic efficiency reflects the deviation of enthalpy change between the real process and the ideal isentropic process. The work consumed by compressor and pump is defined as

$$W_c = \dot{m}(h_{out} - h_{in})/\eta_{is,c}, \quad (1)$$

$$W_p = \dot{m}(h_{out} - h_{in})/\eta_{is,p}. \quad (2)$$

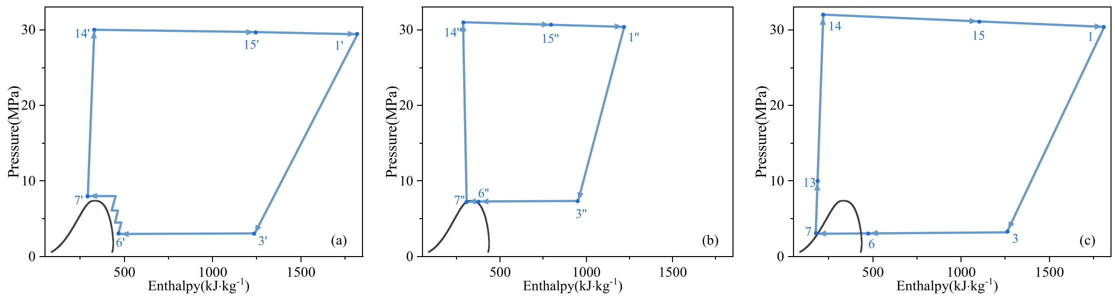

FIG. 2. Pressure-enthalpy diagrams of (a) Allam cycle, (b) Allam-Z cycle, and (c) this work.

The work produced by turbine is calculated as

$$W_t = \dot{m}(h_{in} - h_{out})\eta_{is,t}, \quad (3)$$

where h_{in} and h_{out} represent the enthalpy of the working fluid at the inlet and outlet of each component, and $\dot{m}$ represents the flow rate of the working fluids.

In terms of heat exchanger, the method of discretization is applied that the sum of heat transfer is the combination of every subsection, as defined in Eq. (4). The fluid is regarded as constant properties in each subsection. All the heat exchangers are counter-flow designed with a reasonable pressure drop

$$Q = UA\Delta T. \quad (4)$$

The process in combustion chamber is assumed as a complete reaction for both fuel and oxidant, and the heat release depends on the LHV of fuel, as shown in Eq. (5). The pressure drop is considered to evaluate the irreversible loss during combustion

$$Q_{comb} = m_{fuel}LHV. \quad (5)$$

The power output of the power cycle and the power consumption of ASU are expressed as

$$W_{out} = (W_{T1} + W_{T2}) - (W_{P1} + W_{P2} + W_{P3} + W_{P4} + W_{P7}), \quad (6)$$

$$W_{ASU} = W_{C1} + W_{C2} + W_{P5} + W_{P6}. \quad (7)$$

The air filter and water separator models are considered as black box in this study, which are worked as removing impurities and water contains in air or circulating fluid, and their working efficiency is assumed as 100%.

B. Turbine cooling flow

Considering that the turbine inlet temperature needs to be limited under an allowable value due to the blade material resistance, which is 860 °C,[33,34] for common rotor rows. A specific proportion of CO_2 stream is considered as cooling flow, which is separated from the mainstream after CO_2 capture. The method to determine coolant CO_2 proportion has been extensively studied by scholars, EI-Marsri[35] developed a turbine cooling flow numeric model, based on an assumption that the work is extracted during expanding process continuously, instead of occurring in discrete stages. Thereby, the stator and rotor are regarded as an average stage where the stagnant temperature drops linearly, and the cooling flow rate is expressed as a function of average work extracted from stage. While on the other hand, Horlock and Jones[36] consider the coolant in each stage by the development of the heat transfer model in individual blade, which is closer to the real situation. The authors developed a semi-empirical relation to calculate the amount of cooling stream proportion needed, according to the main gas, cooling air, and metal allowable temperature. In this paper, Horlock's method for blade cooling is adopted:

$$\xi = C\ln(1/(1 - \varepsilon_0)), \quad (8)$$

where ξ is the proportion of cooling flow, and C indicates the "the level of technology," which is suggested taken as 0.03 for conventional cooling fluids. ε_0 is so-called overall cooling effectiveness, which is defined as

$$\varepsilon_0 = (T_{gi} - T_{bl})/(T_{gi} - T_{ci}), \quad (9)$$

where T_{gi}, T_{bl}, and T_{ci} represent the temperature of main gas inlet, blade metal, and coolant inlet temperature, respectively. The value of constant number is given by Haseli;[12] he synthesized the published data of supercritical CO_2 turbine cooling and modified the constant value, and then get the following equation:

$$\xi = 0.270 + 0.1443\ln\varepsilon_0. \quad (10)$$

C. Recuperator model

Due to the large variation of the fluids heat capacity and temperature, the recuperator in this study is modeled as two heat exchangers connected in series, rather than a single heat exchanger, as illustrated in Fig. 3. This configuration can handle multiple streams and improve the pinch-point effect.[37] In this work, the exhaust gas exit turbine is cooled in HX1B and HX1A sequentially and send to water separator at the temperature of the HX1A outlet. Heat from the air separation unit (ASU) is transferred to HX1B and HX1A after each stage of air compression, through a intermediate fluid of Dowtherm-A type thermal oil. A buffer tank is configured to adjust the thermal oil flow rate when air compressor operated in an off-design mode. The temperature difference of each heat exchanger is assumed as 20 K.

D. Air compressor off-design characteristic

In this work, the centrifugal air compressor model is adopted. Different with compressor working under design condition with constant speed, the isentropic efficiency under off-design working condition may deviated from design efficiency. Therefore, an off-design centrifugal air compressor map proposed by Zhang and Cai[38] is adopted here, and the formula for pressure ratio and isentropic

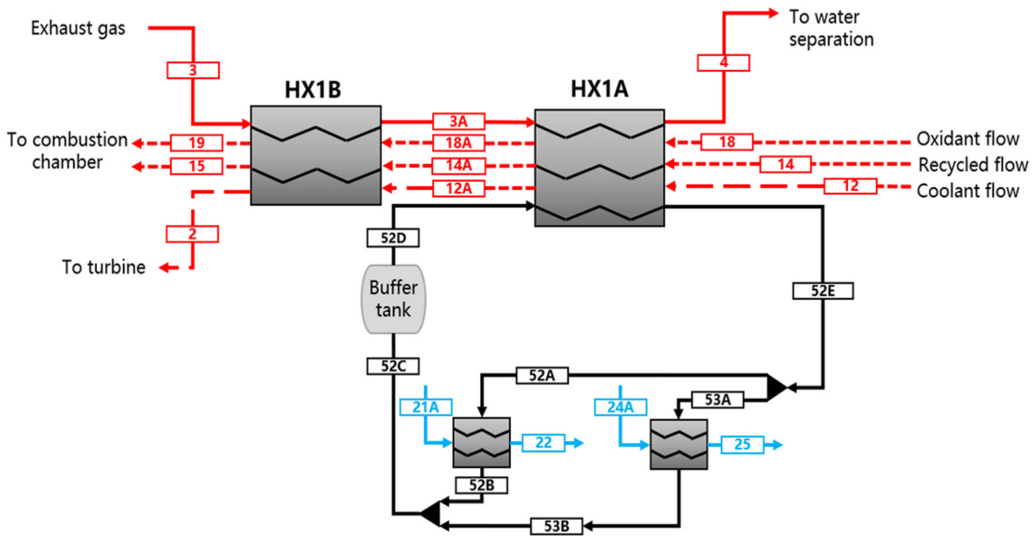

FIG. 3. Schematic diagram of the recuperator model.

efficiency under off-design condition are presented in the following equations:

$$\beta_i/\beta_{i,0} = c_1\dot{m}_c^2 + c_2\dot{m}_c + c_3, \tag{11}$$

$$\eta_i/\eta_{i,0} = [1 - c_4(1-\dot{n}_c)^2](\dot{n}_c/\dot{m}_c)(2-\dot{n}_c/\dot{m}_c), \tag{12}$$

where $\dot{n}_c$ and $\dot{m}_c$ denote the relative speed and mass flow, which is defined as

$$\dot{n}_c = \bar{n}_c/\bar{n}_{c,0}, \tag{13}$$

$$\dot{m}_c = \bar{m}_c/\bar{m}_{c,0}, \tag{14}$$

$$\bar{n}_c = n_c/\sqrt{T_{in}}, \tag{15}$$

$$\bar{m}_c = m_c\sqrt{T_{in}}/p_{in}. \tag{16}$$

c_1–c_4 are the coefficient that are calculated as

$$c_1 = \dot{n}_c/[p(1-m/\dot{n}_c) + \dot{n}_c(\dot{n}_c - m)^2], \tag{17}$$

$$c_2 = (p - 2m\dot{n}_c^2)/[p(1-m/\dot{n}_c) + \dot{n}_c(\dot{n}_c - m)^2], \tag{18}$$

$$c_3 = -(pm\dot{n}_c - m^2\dot{n}_c^3)/[p(1-m/\dot{n}_c) + \dot{n}_c(\dot{n}_c - m)^2]. \tag{19}$$

$c_4 = 0.3$, where both p and m were taken as 1.8.[39] According to above equations, the dynamic characteristic could be determined, and the corresponding characteristic maps are depicted in Fig. 4.

E. Method

The modeling process is developed based on the ASPEN V10 platform licensed by ASPEN TECH and using MATLAB to deliver instructions and call response when different working condition is employed, the properties of working fluid are determined by Peng–Robinson equation, several assumptions are listed below, and further detailed information is shown in Table I.

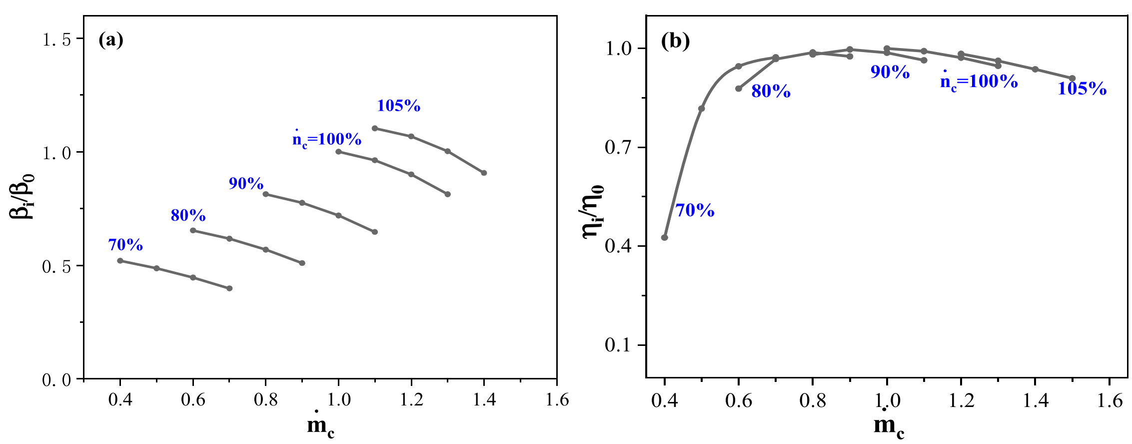

FIG. 4. ASU air compressor characteristic map of (a) pressure ratio and (b) isentropic efficiency.

TABLE I. Previous assumption and working condition.

Items	Value	Ref.
Methane LHV (kJ/kg)	50 010	46
Oxidant flow pressure (MPa)	10	3
Air compressor isentropic efficiency (%)	72	43
Turbine isentropic efficiency (%)	89	47
Pump isentropic efficiency (%)	85	37
Mechanical efficiency (%)	98	37
Generator efficiency (%)	99	48
Environmental temperature (K)	293.15	
HPC operating pressure (MPa)	0.58	43
LPC operating pressure (MPa)	0.13	43

(1) The power cycle is operating in a steady state.[40]
(2) The LNG is assumed as pure methane.[41,42]
(3) The composition of air is considered as 76.5 mol. % nitrogen, 20.5 mol. % oxygen, 1 mol. % argon, and 2 mol. % water.[43]
(4) The pressure drop in heat exchangers is considered as 2% while is ignored in pipeline.[44,45]

F. Economic evaluation model

The economic model net present value (NPV) is adopted in this chapter to further evaluate the cost-effective characteristic of the integrated system, the sensitivity analysis is conducted, and the maximum profitability condition is determined. The mathematic formula of NPV is defined in Eq. (20), where plant lifetime N and interest rate i are 20[49] and 6%,[50] respectively.

$$NPV = -TCI + \left(\sum_{y=1}^{N} \frac{A_y + R_y - E_y - OM_y - F_y}{(1+i)^y} \right). \tag{20}$$

The total investment cost (TCI) consists of direct cost (DC) and indirect cost (IDC), the items of TCI are listed in Table II, and the equipment cost are calculated according to equations[51–56] in supplementary material Table S1.

TABLE II. Content and calculation method of TCI.[57]

Items	Equations
Direct cost	
Equipment cost	$\sum C_i$
Equipment installation	$0.33 \cdot \sum C_i$
Piping	$0.35 \cdot \sum C_i$
Electrical equipment and materials	$0.13 \cdot \sum C_i$
Land	$0.05 \cdot \sum C_i$
Civil, structural, and architectural work	$0.21 \cdot \sum C_i$
Service facilities	$0.35 \cdot \sum C_i$
Indirect cost	
Engineering and supervision	$0.08 \cdot DC$
Construction cost including contractor's profit	$0.15 \cdot DC$
Contingencies	$0.15 \cdot 1.23 \cdot DC$

E_y and A_y represent the yearly revenue by selling electricity and air product, which are defined as

$$E_y = W_{net} \cdot P_{peak} \cdot 3000, \tag{21}$$

$$A_y = (m_{O_2} \cdot P_{O_2} + m_{N_2} \cdot P_{N_2}) \cdot 8760, \tag{22}$$

where the P_{peak}, P_{O_2}, and P_{N_2} represent the price of peak electricity, gaseous oxygen, and gaseous nitrogen. The annual operating hour of Allam cycle is assumed as 3000 h, while the ASU is operating all year.

The annual revenue obtained by LNG regasification service R_y is another part of total income in the LNG terminal,[58] and the value adopted in this paper is 0.028 \$/N m^3, which is the profit of LNG terminal in Zhejiang, China. F_y represents the fuel cost, which is natural gas that paid for combustion.

The OM_y denotes the cost caused by annual maintenance, insurance labor, and plant electricity, which is defined in Eq. (23), and the value assumed for the index is presented in Table III,

$$OM_y = maint_y + lab_y + ins_y. \tag{23}$$

G. Model validation

The model validation of the proposed integrated system is conducted in divided subsections independently. Both Allam cycle and air separation unit showed an acceptable error, with the maximum value of 2.19%, as listed in Table IV. The validation results showed a good accuracy and thereby the method adopted in present work is proved that can predict the state parameters precisely.

IV. RESULTS AND DISCUSSION

A. Thermodynamic analysis

In this chapter, the effect of important parameters on system performance is analyzed, to determine optimum working condition and explore optimization strategies. In addition to the LNG supply flow rate, pressure ratio and water separation temperature are chosen as key parameters to evaluate system thermodynamic performances. Owing to that ASU is integrated with Allam cycle by heat input during air compression process, there are two system efficiency calculation methods; the cycle thermal efficiency evaluates the Allam cycle efficiency considering the external energy input as supplement heat input, while the system electrical efficiency considers the air compression process as extra work consumption. These two definitions are present in Eqs. (24) and (25), respectively,

TABLE III. The economic index assumptions.

Items	Value	Ref.
Fuel cost (\$/GJ)	8.588	52
Annual maintenance cost rate (%)	6	57
Annual insurance cost rate (%)	1	51
Annual labor cost (\$)	20∗40000	51
Peak electricity price (\$/kWh)	0.15	57
Gaseous oxygen price (\$/kg)	0.03019	59
Gaseous nitrogen price (\$/kg)	0.02973	59

TABLE IV. Model validation results of Allam cycle and ASU.

Items	Ref.	This work	Error (%)
Allam cycle[37]			
Natural gas LHV (MJ/kg)	46.50	46.50	0
Turbine inlet temperature (°C)	1150.00	1147.77	0.19
Turbine discharge pressure (MPa)	3.40	3.35	1.47
Turbine outlet temperature (°C)	741.20	741.10	0
Turbine power output (MW)	622.42	608.71	2.19
NG compression work (MW)	4.18	4.15	0.72
Net power output (MW)	419.31	412.58	1.61
Cooling flow temperature (°C)	183.00	182.85	0.08
CO_2 cooling temperature (°C)	26.00	25.78	0.85
ASU[43]			
LNG supply flow (kg/h)	6000	6020	0.33
Air compression work (MW)	36.40	36.88	1.32
Oxygen composition of distillation air (%)	21.00	20.92	0.38
Nitrogen composition of distillation air (%)	78.00	78.06	0.08
Argon composition of distillation air (%)	1.00	1.02	2.00
Produced oxygen purity (%)	99.00	99.99	1.00
Produced oxygen temperature (°C)	−177.97	−177.90	0.04
Produced nitrogen purity (%)	99.00	99.99	1.00
Produced nitrogen temperature (°C)	−193.34	−193.39	0.03

$$\eta_{th} = \frac{W_{net}}{m_{fuel} \cdot LHV + \Delta H_{air}}, \tag{24}$$

$$\eta_e = \frac{W_{net} - W_c}{m_{fuel} \cdot LHV}. \tag{25}$$

As presented in Fig. 5, due to the expansion power output raises faster than pumped work consumed when pressure ratio increase, the thermal and electrical efficiency showed a both raise trend. On the opposite, higher water separation temperature will exhibit lower system efficiency, as the lower water separation temperature enables more exhaust heat regenerated in recuperator and less heat loss happened in water separator. Therefore, enlarge pressure ratio and decline water separation temperature are effective methods to raise system efficiency. However, lower back pressure leads to a lower pressure environment in water separator, which increases the water separation process difficulties. The analyses results show that electrical efficiency is normally 8% lower than thermal efficiency, a bit higher than published results for the reason for lower isentropic efficiency adopted in air compressor model.

The recuperator heat duty distribution map is shown in the bar chart of Fig. 6; the total heat duty of recuperator is reduced with higher pressure ratio, owing to lower turbine exhaust gas temperature under higher expansion ratio. Although the proportion of heat integration from ASU decreases with lower pressure ratio, the amount of heat integration has an increasing trend, which could be explained by the effect of dissimilar heat capacity of cold and hot side in recuperator;[60,61] the heat capacity of low-pressure CO_2 stream is larger than high-pressure CO_2 stream, and this effect is more obvious with larger pressure difference. Therefore, more external heat is needed to match the regenerate temperature at higher pressure ratio. While water separation temperature has no influence on total heat duty but on distribution of ASU and regenerate heat. With lower water separation temperature, integrated heat from ASU showed a decrease trend, considering that more exhaust heat has been recovered when exhaust gas with lower temperature is extracted from recuperator.

B. Economic analysis

Figures 7 and 8 illustrate the cost and revenue distribution of the integrated system, and it can be observed from Fig. 7 that the most significant component is electricity cost, taking over 58% of yearly total cost; it is reasonable as the air separation unit consumes massive electricity with a daily air production of 9935 t; hence, the integrated power cycle could reduce annual cost effectively by electricity supply. The followed composition of cost is main equipment investment, fuel cost, operating and maintenance cost, and insurance cost. Unlike other power systems, which have much larger fuel cost proportion, the

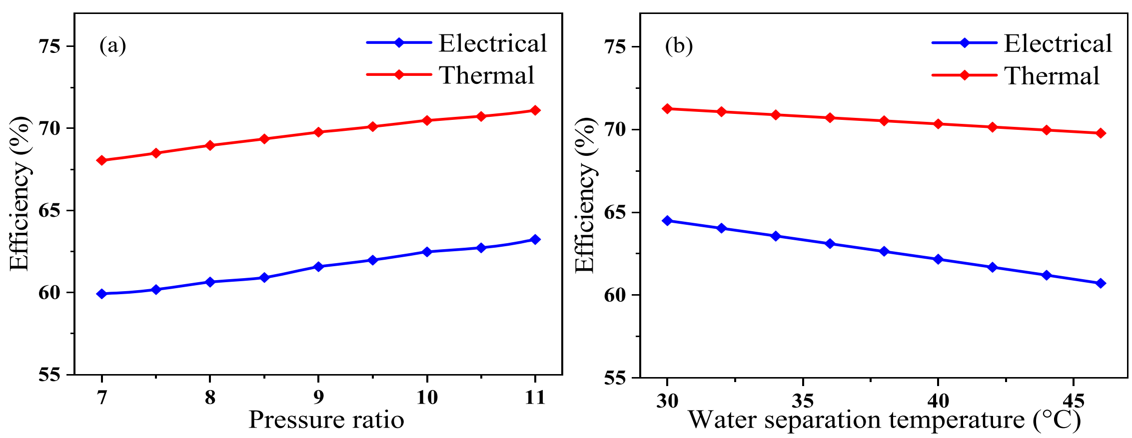

FIG. 5. System efficiency variation with (a) pressure ratio and (b) water separation temperature.

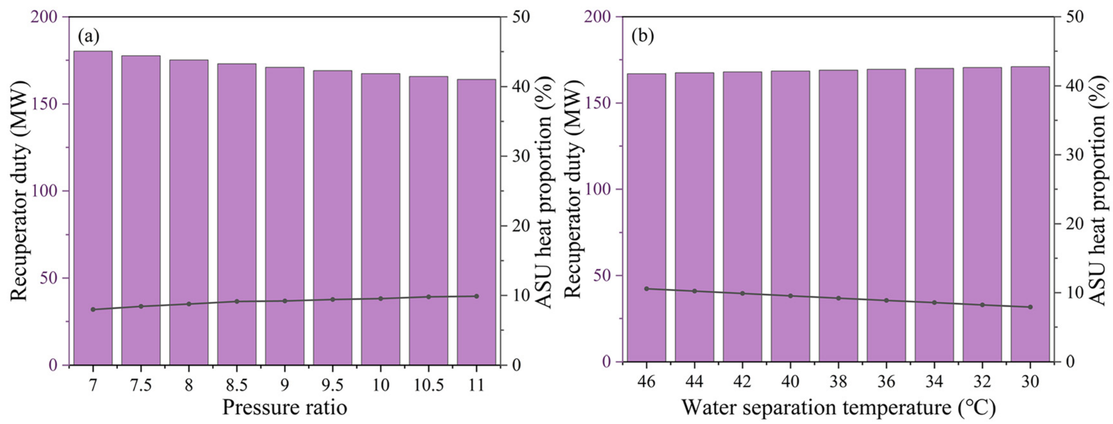

FIG. 6. Recuperator heat duty distribution varied with (a) pressure ratio and (b) water separation temperature.

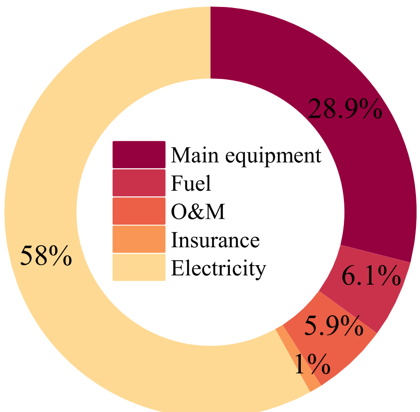

FIG. 7. Integrated system annual cost composition.

composition in this work only takes 6.1% of total cost because the power system has higher efficiency and relatively smaller power scale.

In terms of yearly revenue, as depicted in Fig. 8, the profit from regasification service only takes a tiny proportion, while 99.5% of total revenue come from selling air product , argon product is not considered because system complexity and investment will increase a lot when an argon distillation module is implemented, which could not generate much revenue due to the low content in air.[59]

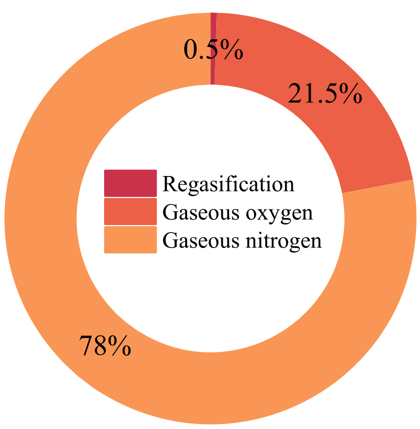

FIG. 8. Integrated system annual revenue composition.

Figure 9 presents integrated system NPV as the function of turbine pressure ratio and oxygen distribution pressure. According to Fig. 9(a), there is a raise trend of NPV value when the pressure ratio increases. Although higher pressure ratio leads to more fuel cost and turbine investment, better thermodynamic performance exhibited and increasingly electricity produced from power cycle, which reduces overall electricity purchase fee and enables better economic performance. In terms of oxygen pressure, which is the distribution pressure at the outlet of T4, may varied with different application. For instance, it is 1.6–3 MPa for steel enterprises[62] and 3.5–10 MPa for oxy-fuel power plant.[63,64] Lower oxygen pressure in power system enables more expansion work and then allows more system economic benefits by reducing system electricity purchase fee.

C. Off-design operating evaluation

In this section, the integrated system operating performance is analyzed based on off-design air compressor characteristic; the design LNG supply flow rate is set as 9.23 kg/s, and the speed variation operating strategy is developed to offset LNG supply flow fluctuation. When LNG supply flow decreases from design value, more compression work is needed to maintain the sub-cooling state of air before entering distillation column, which is achieved by speed up compressor rotor and producing higher air pressure. Varied pressure of air is throttled to distillation column working pressure to enable a steady-state working condition during distillation process. Figure 10 illustrates the energy consumption curve; 87% to 100% speed variation range is determined to meet the −13% to 9% LNG regasification flow fluctuation. During LNG over supply period, there is no obvious change of compression work as the cold energy input is sufficient to produce liquid air, more excess LNG allows more liquid air to be developed, hence, the throttle valve is adjusted to 100% open. On the other hand, compression work increased from 312 to 602 MW when LNG is in short supply of 10%, and the variation of throttling loss reflects the amount of insufficient cold energy of LNG. 58 MW of cold energy short supply can lead to 134 MW electricity input to the ASU, and the

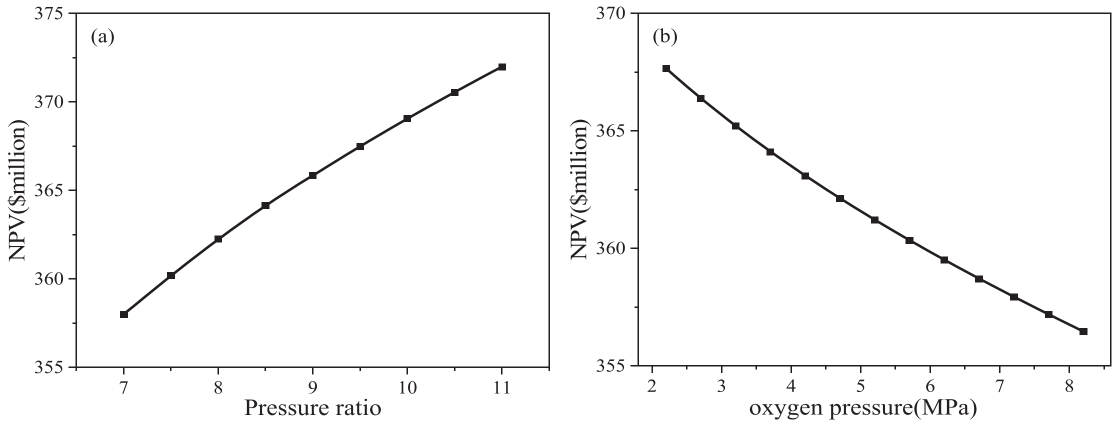

FIG. 9. NPV value variation with (a) pressure ratio and (b) oxygen pressure.

gap becomes more significant with larger deviation from design LNG supply flow rate. Hence, it is costly when operating the system under long-term shortage of LNG supply flow.

D. Case results

According to the thermodynamic analysis, the thermodynamic parameters of the system are listed in Tables VI and VII. The water separation temperature is set as 33.5 °C for easier water condensation and system efficiency enhancement and maintains the temperature difference at HX1 outlet at the same value with other heat exchanger, which is the design temperature difference of 20 K. The pressure ratio of gas turbine is set as 9.69, where the working fluids is expanded from 31 to 3.2 MPa. High pressure atmosphere combustion technology and water separation in low-pressure environment is the main handicap to develop higher pressure ratio. The Allam cycle has net power output of 38.50 MW; meanwhile, the LNG-LO_2 cascaded cold energy utilization method could exhibit high thermal efficiency and electrical efficiency of 70.93% and 63.68%, respectively. The net present value reaches $403.63 million, with the main profit coming from air product. Further decrease in electricity cost could achieve higher NPV value. The power scale of the Allam cycle is the maximum under present ASU production and operating mode, as the cold energy of distillate LO_2 is totally utilized by Allam cycle.

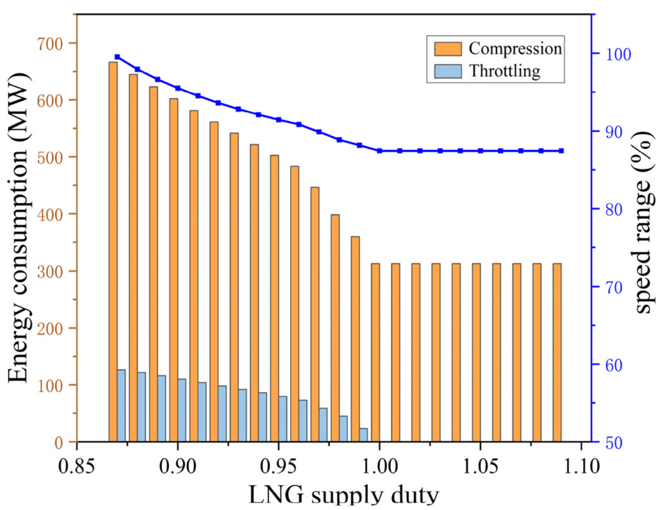

FIG. 10. Energy consumption of the off-design air compressor.

In order to further verify the superiority of the proposed integrated system, the conventional Allam-LNG cycle is modeled here, which directly utilize LNG cold energy as heat sink in Allam cycle. The comparison results between two Allam cycles are listed in Table V. The Allam cycle with improved LNG cold energy utilization method could exhibit higher power output, as oxygen production could supply larger cold energy than LNG. The work consumption of ASU is nearly the same in two Allam cycles, considering that the cold energy of produced liquid oxygen is recovered in main heat exchanger while the cold energy input is implemented by the LNG in proposed system. Moreover, the proposed system outperforms significant thermodynamic performance improvements, and the thermal and electrical efficiency increased by 5.76% and 6.48%, respectively. Therefore, the reduced fuel cost and declined electricity cost is enabled and leads to a 11.0% improvement of net present value.

V. CONCLUSIONS

In this paper, the whole process of Allam cycle-ASU integrated system is simulated, and an improved LNG cold energy utilization method is proposed; key parameters influence on the whole system is investigated based on thermodynamic and economic analyses, and the system off-design operating performance is evaluated. The main conclusions are summarized as followed:

TABLE V. Performance comparison with conventional Allam cycles.

Items	This work	Allam-LNG
LNG supply flow (kg/s)	9.23	9.23
Air production flow rate (t/d)	9935	9935
ASU power consumption (MW)	44.46	44.51
Power cycle output (MW)	38.50	20.96
Thermal efficiency (%)	70.93	65.17
electrical efficiency (%)	63.68	57.20
Net present value ($ million)	403.63	363.64

(1) The modified integrated Allam cycle-ASU system combined with LNG/LO_2 cold energy is modeled. The power cycle could maintain steady operation based on our improved LNG cold energy utilization method that transfers cold energy to LO_2 through ASU. According to the proposed system, an ASU with 9935 t/d air production could support 38.50 MW of cold energy utilization Allam cycle.
(2) A comprehensive thermodynamic and economic analyses is conducted; the impact of key parameters including pressure ratio, water separation temperature, and oxygen expansion pressure is investigated in respect of operating efficiency, heat integration performance, and economic benefits.
(3) The optimal working condition of the proposed system is determined, which delivers thermal and electrical efficiency of 70.93% and 63.68%, which is 5.76% and 6.48% higher than conventional Allam-LNG cycle. In addition, the NPV value achieves $403.63 million, increased by 11.0% compared with Allam-LNG cycle.
(4) The air compressor off-design characteristic is invested, and the working performance is analyzed; a −13% to 9% range of LNG supply fluctuated could be adjusted when develop the speed variation range between 87% and 100%.

SUPPLEMENTARY MATERIAL

See the supplementary material for system main components cost functions.

ACKNOWLEDGMENTS

This work was supported by the National Natural Science Foundation of China under Grant No. 52325605, the Zhejiang Provincial Natural Science Foundation under Grant No. LR20E060001, and the Fundamental Research Funds for the Central Universities under Grant No. 2022ZFJH04.

AUTHOR DECLARATIONS

Conflict of Interest

The authors have no conflicts to disclose.

Author Contributions

Yi Wu: Conceptualization (equal); Data curation (equal); Investigation (equal); Methodology (equal); Software (equal); Validation (equal); Writing – original draft (equal). **Zheng Wang:** Conceptualization (equal); Investigation (equal); Methodology (equal). **Yafei Liu:** Data curation (equal); Investigation (equal). **Qinghe Guo:** Data curation (equal); Investigation (equal). **Zhangquan Wen:** Data curation (equal); Investigation (equal). **Dan Chen:** Data curation (equal); Investigation (equal). **Kaigang Gong:** Data curation (equal); Investigation (equal). **Peiwang Zhu:** Methodology (equal); Resources (equal); Supervision (equal); Writing – review & editing (equal). **Gang Xiao:** Methodology (equal); Resources (equal); Supervision (equal); Writing – review & editing (equal).

DATA AVAILABILITY

The data that support the findings of this study are available from the corresponding author upon reasonable request.

APPENDIX: STREAM POINT PARAMETERS

Stream state point parameters of the integrated system. Stream state point parameters of the recuperator.

TABLE VI. Stream state point parameters of the integrated system.

State point	m (kg s^{-1})	T (°C)	P (MPa)	State point	m (kg s^{-1})	T (°C)	P (MPa)
1	74.91	1150.07	30.38	26	0.68	30.00	0.62
2	8.36	250.00	30.73	27	113.56	30.00	0.62
3	83.27	722.67	3.20	28	113.56	−172.22	0.61
4	83.27	33.47	3.14	29	36.32	−172.22	0.61
5	2.17	33.47	3.07	30	43.75	−177.11	0.58
6	81.10	33.47	3.07	31	43.75	−180.50	0.57
7	81.10	−10.00	3.01	32	77.24	−172.22	0.61
8	2.65	−10.00	3.01	33	69.80	−172.80	0.60
9	78.46	−10.00	3.01	34	69.80	−180.50	0.59
10	78.46	−3.96	10.00	35	86.16	−193.38	0.13
11	8.36	−3.96	10.00	36	86.16	−178.17	0.12
12	8.36	13.21	32.00	37	86.16	−15.00	0.11
13	37.81	−3.96	10.00	38	2.61	−185.68	0.13
14	37.81	13.21	32.00	39	2.61	−15.00	0.12
15	37.81	703.22	30.73	40	24.79	−177.90	0.17
16	32.29	−3.96	10.00	41	72.38	−174.07	10.20
17	36.14	−2.87	10.00	42	72.38	13.56	10.00
18	36.14	12.58	32.00	43	68.53	13.56	10.00
19	36.14	703.22	30.73	44	68.53	−83.99	2.20
20	115.00	25.00	0.10	45	3.85	13.56	10.00
21	115.00	25.00	0.10	46	9.23	−162.00	0.13
22	115.00	40.00	0.45	47	0.96	−147.64	33.00
23	0.76	30.00	0.45	48	8.27	−159.34	6.12
24	114.24	30.00	0.45	49	8.27	−15.00	6.00
25	114.24	40.00	0.62	50	0.96	−15.00	32.34
				51	0.96	5.00	31.69

TABLE VII. Stream state point parameters of the recuperator.

State point	m (kg s^{-1})	T (°C)	P (MPa)	State point	m (kg s^{-1})	T (°C)	P (MPa)
2	8.36	250.00	30.73	19	36.14	703.22	30.73
3	83.27	722.67	3.20	21A	115.00	233.34	0.46
3A	83.27	206.71	3.14	22	115.00	40.00	0.45
4	83.27	33.47	3.14	24A	115.00	69.13	0.63
12	8.36	13.21	32.00	25	114.24	40.00	0.62
12A	8.36	186.71	31.36	52A	72	20.00	0.39
14	37.81	13.21	32.00	52B	72	213.57	0.38
14A	37.81	186.71	31.36	52C	75.62	206.71	0.38
15	37.81	703.22	30.73	52D	4.77	206.71	0.38
18	36.14	12.58	32.00	52E	75.62	33.47	0.37
18A	36.14	186.71	31.36	53A	3.62	20	0.37
				53B	3.62	49.27	0.37

NOMENCLATURE

Terminology

h	Specific enthalpy (MJ/kg^{-1})
m	Mass flow (kg/s)
P	Price (\$)
p	Pressure (MPa)
T	Temperature (°C)
$\Delta\bar{T}$	Logarithmic mean temperature difference (K)
UA	Total conductance of heat exchanger (MW/K^{-1})
V	Volume (m^3)
W	Power (MW)
η	Efficiency

Abbreviations

ASU	Air separation unit
DC	Direct cost
LHV	Lower heating value
LNG	Liquefied natural gas
LO_2	Liquefied oxygen
NG	Natural gas
NPV	Net present value
sCO_2	Supercritical CO_2
TCI	Total cost investment

Subscripts

c	Compressor
$comb$	Combustion
e	Electrical
f	Fuel
g	Generator
in	Inlet
is	Isentropic process
net	Net output
out	Outlet
p	Pump
t	Turbine
th	Thermal
y	Yearly
0	Design value

REFERENCES

[1]IEA, see https://www.iea.org/reports/co2-emissions-in-2022 for "CO_2 emissions in 2022" (2023).

[2]S. Yadav and S. S. Mondal, "A review on the progress and prospects of oxy-fuel carbon capture and sequestration (CCS) technology," Fuel **308**, 122057 (2022).

[3]R. Allam, S. Martin, B. Forrest, J. Fetvedt, X. J. Lu, D. Freed, G. W. Brown, T. Sasaki, M. Itoh, and J. Manning, "Demonstration of the Allam Cycle: An update on the development status of a high efficiency supercritical carbon dioxide power process employing full carbon capture," Energy Procedia **114**, 5948–5966 (2017).

[4]L. Colleoni, A. Sindoni, and S. Ravelli, "Comprehensive thermodynamic evaluation of the natural gas-fired Allam cycle at full load," Energies **16**(6), 2597 (2023).

[5]A. Rogalev, N. Rogalev, V. Kindra, O. Zlyvko, and A. Vegera, "A study of low-potential heat utilization methods for oxy-fuel combustion power cycles," Energies **14**(12), 3364 (2021).

[6]C. Peng, C. Zou, J. X. Ren, Q. J. Lin, W. X. Xia, J. H. Luo, and Y. Y. Xiao, "Ignition delay times of C_2H_4, C_2H_4/n-C_4H_{10}, and n-C_4H_{10}/i-C_4H_{10} under O_2/CO_2 atmospheres: Shock tube experiments and kinetic model," Combust. Flame **254**, 112825 (2023).

[7]R. Zhao and D. Liu, "Chemical effects of carbon dioxide in ethylene, ethanol and DME counter-flow diffusion flames: An experimental reference for the fictitious CO_2 flame," J. Energy Inst. **100**, 245–258 (2022).

[8]D. Qi, M. Chen, K. Yang, T. Li, Y. Ying, and D. Liu, "Effective reduction on flame soot via plasma coupled with carbon dioxide," J. Hazard. Mater. **466**, 133669 (2024).

[9]M. Chen, D. Liu, and B. Jiang, "Soot formation and combustion characteristics in confined mesoscale combustors under conventional and oxy-combustion conditions (O_2/N_2 and O_2/CO_2)," Fuel **264**, 116808 (2020).

[10]C. Chen, Q. Yang, R. Zhang, and D. Liu, "Regulation of organic hydrocarbon pollutants in coal volatiles combustion with CO_2 addition," J. Cleaner Prod. **374**, 133904 (2022).

[11]A. Ebadi, A. Saraei, H. Mohsenimonfared, and S. J. Mehrabadi, "Thermoeconomic analysis of combined steam and organic Rankine cycle with primary mover of Allam cycle," Int. J. Energy Environ. Eng. **13**(1), 231–239 (2022).

[12]Y. Haseli and N. S. Sifat, "Performance modeling of Allam cycle integrated with a cryogenic air separation process," Comput. Chem. Eng. **148**, 107263 (2021).

[13]J. M. Amann, M. Kanniche, and C. Bouallou, "Natural gas combined cycle power plant modified into an O_2/CO_2 cycle for CO_2 capture," Energy Convers. Manage. **50**(3), 510–521 (2009).

[14]D. Fernandes, S. Wang, Q. Xu, and D. Chen, "Dynamic simulations of the Allam cycle power plant integrated with an air separation unit," Int. J. Chem. Eng. **2019**, 6035856.

[15]S. A. Zaryab, R. Scaccabarozzi, and E. Martelli, "Advanced part-load control strategies for the Allam cycle," Appl. Therm. Eng. **168**, 114822 (2020).

[16]W. Chan, X. L. Lei, F. C. Chang, and H. X. Li, "Thermodynamic analysis and optimization of Allam cycle with a reheating configuration," Energy Convers. Manage. **224**, 113382 (2020).

[17]M. N. Xie, L. X. Chen, K. Wu, Z. K. Liu, J. Lin, C. X. Jiang, S. Xie, and Y. R. Zhao, "A novel peak shaving approach to improving load flexibility of the Allam cycle by integrating cold energy storage," J. Cleaner Prod. **386**, 135769 (2023).

[18]M. N. Xie, S. L. Liu, L. X. Chen, Y. N. Zhang, Y. T. Wang, S. Xie, and Y. R. Zhao, "Techno-economic and environmental assessment of a novel co-generation system integrating heat pump with Allam cycle," Energy Convers. Manage. **277**, 116606 (2023).

[19]E. Dokhaee, A. Saraei, H. Mohsenimonfared, and P. Yousefi, "Exergy and thermoeconomic analysis of a combined Allam generation system and absorption cooling system," Int. J. Energy Environ. Eng. **13**(1), 267–273 (2021).

[20]J. Luo, O. Emelogu, T. Morosuk, and G. Tsatsaronis, "Exergy-based investigation of a coal-fired allam cycle," Energy **218**, 119471 (2021).

[21]T. T. Xin, C. Xu, Y. H. Liu, and Y. P. Yang, "Thermodynamic analysis and economic evaluation of a novel coal-based zero emission polygeneration system using solar gasification," Appl. Therm. Eng. **201**, 117814 (2022).

[22]Z. L. Zhu, Y. P. Chen, J. F. Wu, S. B. Zhang, and S. X. Zheng, "A modified Allam cycle without compressors realizing efficient power generation with peak load shifting and CO_2 capture," Energy **174**, 478–487 (2019).

[23]Y. D. Fu, L. Cai, R. Yan, and Y. W. Guan, "Thermodynamic analysis of the biomass gasification Allam cycle," Fuel **350**, 128781 (2023).

[24]Y. Y. Li, Y. J. Liu, G. Q. Zhang, and Y. P. Yang, "Thermodynamic analysis of a novel combined cooling and power system utilizing liquefied natural gas (LNG) cryogenic energy and low-temperature waste heat," Energy **199**, 117479 (2020).

[25]Z. X. Sun, F. Q. Xu, S. J. Wang, J. P. Lai, and K. Lin, "Comparative study of Rankine cycle configurations utilizing LNG cold energy under different NG distribution pressures," Energy **139**, 380–393 (2017).

[26]J. Ma, X. D. Song, B. Zhang, N. Mao, and T. B. He, "Optimal design of dual-stage combined cycles to recover LNG cold energy and low-temperature waste thermal energy for sustainable power generation," Energy Convers. Manage. **269**, 116141 (2022).

[27]J. Y. Wang, J. F. Wang, Y. P. Dai, and P. Zhao, "Off-design performance analysis of a transcritical CO_2 Rankine cycle with LNG as cold source," Int. J. Green Energy **14**(9), 774–783 (2017).

[28]Y. Cao, J. Zhan, Q. Cao, and F. Q. Si, "Techno-economic analysis of cascaded supercritical carbon dioxide combined cycles for exhaust heat recovery of typical gas turbines," Energy Convers. Manage. **258**, 115536 (2022).
[29]H. S. Yu, T. Gundersen, and E. Gencer, "Optimal liquified natural gas (LNG) cold energy utilization in an Allam cycle power plant with carbon capture and storage," Energy Convers. Manage. **228**, 113725 (2021).
[30]W. Chan, H. X. Li, X. Li, F. C. Chang, L. L. Wang, and Z. M. Feng, "Exergoeconomic analysis and optimization of the Allam cycle with liquefied natural gas cold exergy utilization," Energy Convers. Manage. **235**, 113972 (2021).
[31]B. Li, S.-S. Wang, J. F. Qiao, B. B. Wang, and L. M. Song, "Thermodynamic analysis and optimization of a dual-pressure Allam cycle integrated with the regasification of liquefied natural gas," Energy Convers. Manage. **246**, 114660 (2021).
[32]H. F. Lu, M. Azimi, and T. Iseley, "Short-term load forecasting of urban gas using a hybrid model based on improved fruit fly optimization algorithm and support vector machine," Energy Rep. **5**, 666–677 (2019).
[33]J. S. Hong, G. Chaudhry, J. G. Brisson, R. Field, M. Gazzino, and A. F. Ghoniem, "Analysis of oxy-fuel combustion power cycle utilizing a pressurized coal combustor," Energy **34**(9), 1332–1340 (2009).
[34]C. Mitchell, V. Avagyan, H. Chalmers, and M. Lucquiaud, "An initial assessment of the value of Allam cycle power plants with liquid oxygen storage in future GB electricity system," Int. J. Greenhouse Gas Control **87**, 1–18 (2019).
[35]M. A. El-Masri, "On thermodynamics of gas-turbine cycles: Part 2—A model for expansion in cooled turbines," J. Eng. Gas Turbines Power **108**(1), 151–159 (1986).
[36]J. H. Horlock, D. T. Watson, and T. V. Jones, "Limitations on gas turbine performance imposed by large turbine cooling flows," J. Eng. Gas Turbines Power-Trans. ASME **123**(3), 487–494 (2001).
[37]R. Scaccabarozzi, M. Gatti, and E. Martelli, "Thermodynamic analysis and numerical optimization of the NET Power oxy-combustion cycle," Appl. Energy **178**, 505–526 (2016).
[38]N. Zhang and R. X. Cai, "Analytical solutions and typical characteristics of part-load performances of single shaft gas turbine and its cogeneration," Energy Convers. Manage. **43**(9), 1323–1337 (2002).
[39]C. Guo, Y. J. Xu, H. Guo, X. J. Zhang, X. P. Lin, L. Wang, Y. Zhang, and H. S. Chen, "Comprehensive exergy analysis of the dynamic process of compressed air energy storage system with low-temperature thermal energy storage," Appl. Therm. Eng. **147**, 684–693 (2019).
[40]H. W. Choi, S.-I. Na, S. B. H, Y. Chung, D. K. Kim, and M. S. Kim, "Optimal design of organic Rankine cycle recovering LNG cold energy with finite heat exchanger size," Energy **217**, 119268 (2021).
[41]Z. X. Sun, Z. Q. Wu, Q. Z, X. L, and K. L, "Thermodynamic improvements of LNG cold exergy power generation system by using supercritical ORC with unconventional condenser," Energy Convers. Manage. **223**, 113263 (2020).
[42]S.-H. Cha, S.-L. Na, Y. H. Lee, and M. S. Kim, "Thermodynamic analysis of a gas turbine inlet air cooling and recovering system in gas turbine and CO_2 combined cycle using cold energy from LNG terminal," Energy Convers. Manage. **230**, 113802 (2021).
[43]M. H. Hamayun, N. Ramzan, M. Hussain, and M. Faheem, "Conventional and advanced exergy analyses of an integrated LNG regasification-air separation process," Ind. Eng. Chem. Res. **61**(7), 2843–2853 (2022).
[44]X. Wang, L. Zhao, L. H. Zhang, M. H. Zhang, and H. Dong, "A novel combined system for LNG cold energy utilization to capture carbon dioxide in the flue gas from the magnesite processing industry," Energy **187**, 115963 (2019).
[45]I. H. Kim and H. C. No, "Physical model development and optimal design of PCHE for intermediate heat exchangers in HTGRs," Nucl. Eng. Des. **243**, 243–250 (2012).
[46]N. Zhang and N. Lior, "A novel near-zero CO_2 emission thermal cycle with LNG cryogenic exergy utilization," Energy **31**(10–11), 1666–1679 (2006).
[47]G. Q. Zhang, J. Z. Zheng, Y. P. Yang, and W. Y. Liu, "A novel LNG cryogenic energy utilization method for inlet air cooling to improve the performance of combined cycle," Appl. Energy **179**, 638–649 (2016).
[48]Y. M. Zhao, B. Yu, B. Wang, S. J. Zhang, and Y. H. Xiao, "Heat integration and optimization of direct-fired supercritical CO_2 power cycle coupled to coal gasification process," Appl. Therm. Eng. **130**, 1022–1032 (2018).
[49]Y. Zhou, Z. Xu, J. Zhang, J. Xing, J. Jia, and P. Cui, "Development and techno-economic evaluation of coal to ethylene glycol process and Allam power cycle and carbon capture and storage and integration process," Fuel **332**, 126121 (2023).
[50]S. Michalski, D. P. Hanak, and V. Manovic, "Advanced power cycles for coal-fired power plants based on calcium looping combustion: A techno-economic feasibility assessment," Appl. Energy **269**, 114954 (2020).
[51]J.-Q. Guo, M.-J. Li, J.-L. Xu, J.-J. Yan, and T. Ma, "Energy, exergy and economic (3E) evaluation and conceptual design of the 1000 MW coal-fired power plants integrated with S-CO_2 Brayton cycles," Energy Convers. Manage. **211**, 112713 (2020).
[52]H. Ghaebi, M. Amidpour, S. Karimkashi, and O. Rezayan, "Energy, exergy and thermoeconomic analysis of a combined cooling, heating and power (CCHP) system with gas turbine prime mover," Int. J. Energy Res. **35**(8), 697–709 (2011).
[53]M. Gorji-Bandpy, H. Goodarzian, and M. Biglari, "The cost-effective analysis of a gas turbine power plant," Energy Sources, Part B **5**(4), 348–358 (2010).
[54]Z. Guo-Yan, W. En, and T. Shan-Tung, "Techno-economic study on compact heat exchangers," Int. J. Energy Res. **32**(12), 1119–1127 (2008).
[55]D. Prakash and O. Singh, "Thermo-economic study of combined cycle power plant with carbon capture and methanation," J. Cleaner Prod. **231**, 529–542 (2019).
[56]H. Abbaspour, M. A. Ehyaei, A. Ahmadi, M. Panahi, A. Abdalisousan, and A. Mirzohosseini, "Energy, exergy, economic, exergoenvironmental and environmental (5E) analyses of the cogeneration plant to produce electrical power and urea," Energy Convers. Manage. **235**, 113951 (2021).
[57]L. Zhang and B. Sobhani, "Comprehensive economic analysis and multi-objective optimization of an integrated power and freshwater generation cycle based on flash-binary geothermal and gas turbine cycles," J. Cleaner Prod. **364**, 132644 (2022).
[58]D. Fioriti, A. Baccioli, G. Pasini, A. Bischi, F. Migliarini, D. Poli, and L. Ferrari, "LNG regasification and electricity production for port energy communities: Economic profitability and thermodynamic performance," Energy Convers. Manage. **238**, 114128 (2021).
[59]A. F. Young, H. G. D. Villardi, L. S. Araujo, L. S. C. Raptopoulos, and M. S. Dutra, "Detailed design and economic evaluation of a cryogenic air separation unit with recent literature solutions," Ind. Eng. Chem. Res. **60**(41), 14830–14844 (2021).
[60]F. Crespi, G. Gavagnin, D. Sánchez, and G. S. Martínez, "Supercritical carbon dioxide cycles for power generation: A review," Appl. Energy **195**, 152–183 (2017).
[61]K. Wang, Y.-L. He, and H.-H. Zhu, "Integration between supercritical CO_2 Brayton cycles and molten salt solar power towers: A review and a comprehensive comparison of different cycle layouts," Appl. Energy **195**, 819–836 (2017).
[62]L. Zhang, Z. Zheng, Z. J. Xu, and Y. Chai, "Optimal scheduling of oxygen system in steel enterprises considering uncertain demand by decreasing pipeline network pressure fluctuation," Comput. Chem. Eng. **160**, 107692 (2022).
[63]S. Deng and R. Hynes, "Thermodynamic analysis and comparison on oxy-fuel power generation process," J. Eng. Gas Turbines Power **131**(5), 053001 (2009).
[64]L. Cai, Y. D. Fu, Z. Y. Cheng, Y. L. Xiang, and Y. W. Guan, "Advanced exergy and exergoeconomic analyses to evaluate the economy of LNG oxy-fuel combined cycle power plant," J. Environ. Chem. Eng. **10**(5), 108387 (2022).